PROCEEDINGS, 50th Workshop on Geothermal Reservoir Engineering
Stanford University, Stanford, California, February 10-12, 2025
SGP-TR-229

Characterization of Drill Core from Hydraulically Stimulated Crystalline Rock Following Hydraulic Fracturing at the Utah FORGE Geothermal Test Site

Clay G. Jones, Stuart S. Simmons and Joseph N. Moore

EGI, University of Utah, Salt Lake City, UT

cjones@egi.utah.edu; ssimmons@egi.utah.edu; jmoore@egi.utah.edu

Keywords: Engineered Geothermal Systems, Hydraulic Stimulation; Crystalline Rocks, Core Through; Natural Fractures, Induced Fractures, Vein Mineralization

ABSTRACT

In April 2022, three hydraulic stimulation stages were completed near the toe of injection well 16A(78)-32. In April-June 2023 the production well, 16B(78)-32, was drilled ~300 ft above and roughly parallel to the highly-deviated injection well. Three intervals in the production well cored through stimulated crystalline reservoir rock, totaling 135.8 ft. Core from stimulation 1 (10,430 to 10,493 ft) and 3 (9,800 to 9,853 ft) consists of dark-colored, banded gneiss. Core from stimulation 2 (10,250 to 10,304 ft) consists of light-colored granitoid. Fractures in the core were assigned the following classifications: 1) planar; 2) semi-planar; 3) unbroken mineralized; 3) rough; 4) concave-convex; and 5) curviplanar. Within individual core runs coherent fracture measurements of planar features (planar, semi-planar and unbroken mineralized fractures) were obtained. Measured fracture orientations were rotated to match the trajectory of the deviated well. A depth correction and an axial rotation was then applied to best fit microresistivity image logs. Planar features dominantly strike NNW-SSE in alignment with the maximum horizontal stress. Planar features were most common in gneiss from the stimulation 1 and 3 cores, with the stimulation 3 core containing most planar features. The stimulation 3 core may have been adjacent to a reactivated natural fracture zone. Fractures containing secondary vein minerals were open and filled with fluid in the reservoir prior to the drilling of 16B(78)-32. The majority of the planar features are mineralized, with calcite being the most common phase. Calcite ± anhydrite may have precipitated from the injected fluids at reservoir temperatures. Cross-cutting relationships suggest closely spaced, curviplanar fractures in the bottom of the stimulation 1 core are impermeable features in the reservoir.

1 INTRODUCTION

Utah FORGE is a field-based, underground laboratory sponsored by the US Department of Energy to develop, test and accelerate breakthroughs in Enhanced Geothermal System (EGS) technologies in order to advance the uptake of non-traditional geothermal resources (Moore et al., 2020, 2023). The centerpiece of the Utah FORGE project is a deep, deviated injection-production well doublet (Figure 1). The injection well, 16A(78)-32 was stimulated in three stages in April 2022. Stage 1 was pumped down the casing to stimulate 200 ft of open hole below the casing string. Stages 2 and 3 were treated through perforations in the casing. A friction reducer was added to stages 1 and 2, and a viscosifier to stage 3 (Jones et al., 2023). The production well, 16B(78)-32 was drilled along the same trajectory as 16A(78)-32, and ~300 ft shallower in the tangent section (Figure 1). Core was cut in May-June 2023, over a year after the three stage stimulation near the toe of 16A(78)-32. Core was recovered from three intervals, one per stimulation stage, in the crystalline rocks that had been impacted by the stimulation of 16A(78)-32 (Figure 2). The core intervals were selected, in large part, based on micro seismic data (Dyer et al., 2023a; 2023b) collected during the stimulation of 16A(78)-32 (Figure 3). Seven core runs were made with 135.8 ft of core recovered (Table 1, Figure 2).

1.1 Characterizing the Core

The core collected from well 16B(78)-32 comes from ≥ 300 ft from the stimulated zones in well 16A(78)-32 and offers a unique opportunity to observe the impact of hydraulic stimulations in crystalline rock. These observations are critical in evaluating what the stimulated fractures in the EGS reservoir look like, by providing the only direct observations of fracture distribution, fracture orientations and secondary mineralization.

1.2 Rock Types

Core from stimulation zones 3 (9,800 to 9,853 ft) and 1 (10,430 to 10,493 ft) consist of fine-grained, dark-colored gneiss with coarser-grained, light-colored felsic bands (Figure 2). Core from stimulation zone 2 (10,250 to 10,304 ft) consists of coarse-grained, moderately-foliated, light-colored granitoid. Rock fabric in the core from stimulations 3 and 1 is oriented similarly to the trajectory of the core axis. This relationship was useful in aligning the core sections within core runs.

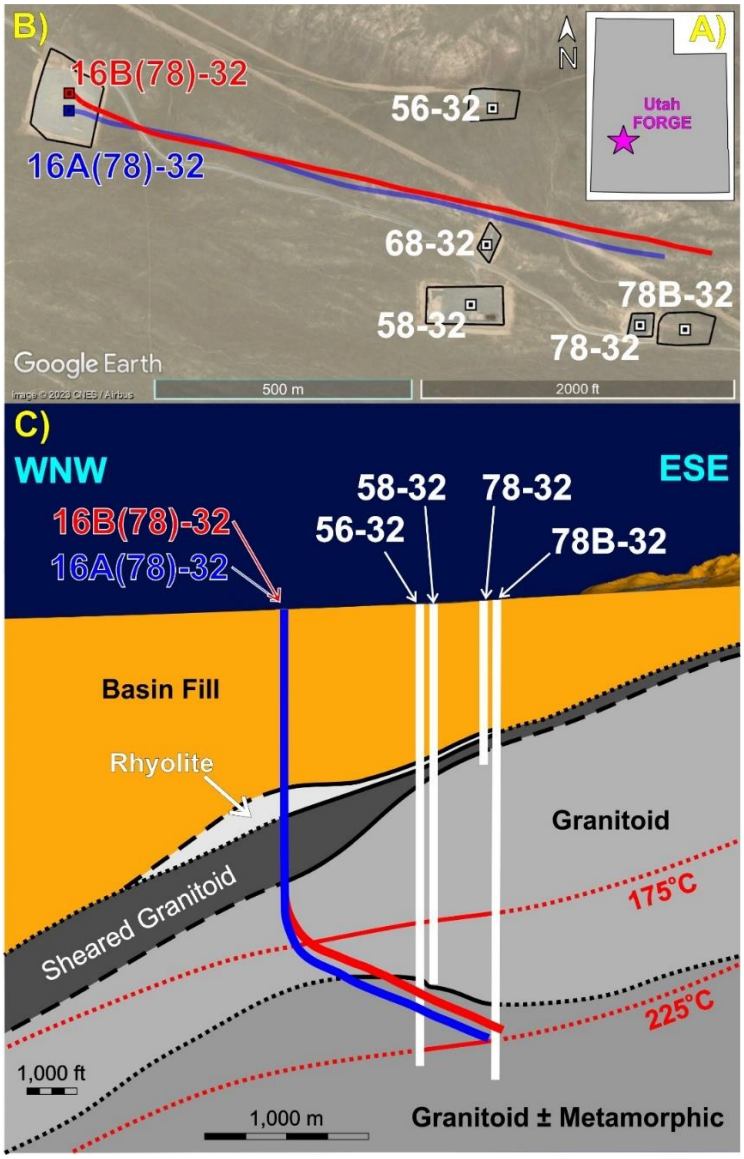

Figure 1: A) The location of the Utah FORGE site within the state of Utah. B) Infield satellite image of the Utah FORGE site showing drill pads, wellhead locations and the surface trajectories of injection well 16A(78)-32 (red) and production well 16A(78)-32 (blue). C) Cross section (1:1) through the FORGE reservoir, along the trajectories of the injection-production wells, showing well trajectories, basic lithologies and temperature contours.

Table 1: Coring summary for tangent core runs 1 through 7 in well 16B(78)-32.

Core Run	Location	Top MD (ft)	Bottom MD (ft)	Cored Length (ft)	Recovery (ft)	Recovery %
1 - tangent	Stim 3	9,800.0	9,817.0	17	16.6	98%
2 - tangent	Stim 3	9,823.0	9,853.0	30	28.4	95%
3 - tangent	Stim 2	10,250.0	10,256.0	6	5.5	92%
4 - tangent	Stim 2	10,264.0	10,272.0	8	4.6	58%
5 - tangent	Stim 2	10,274.0	10,304.0	30	28.0	93%
6 - tangent	Stim 1	10,430.0	10,460.0	30	25.7	86%
7 - tangent	Stim 1	10,462.0	10,493.0	31	27.0	87%
			Totals	**152.0**	**135.8**	**89%**

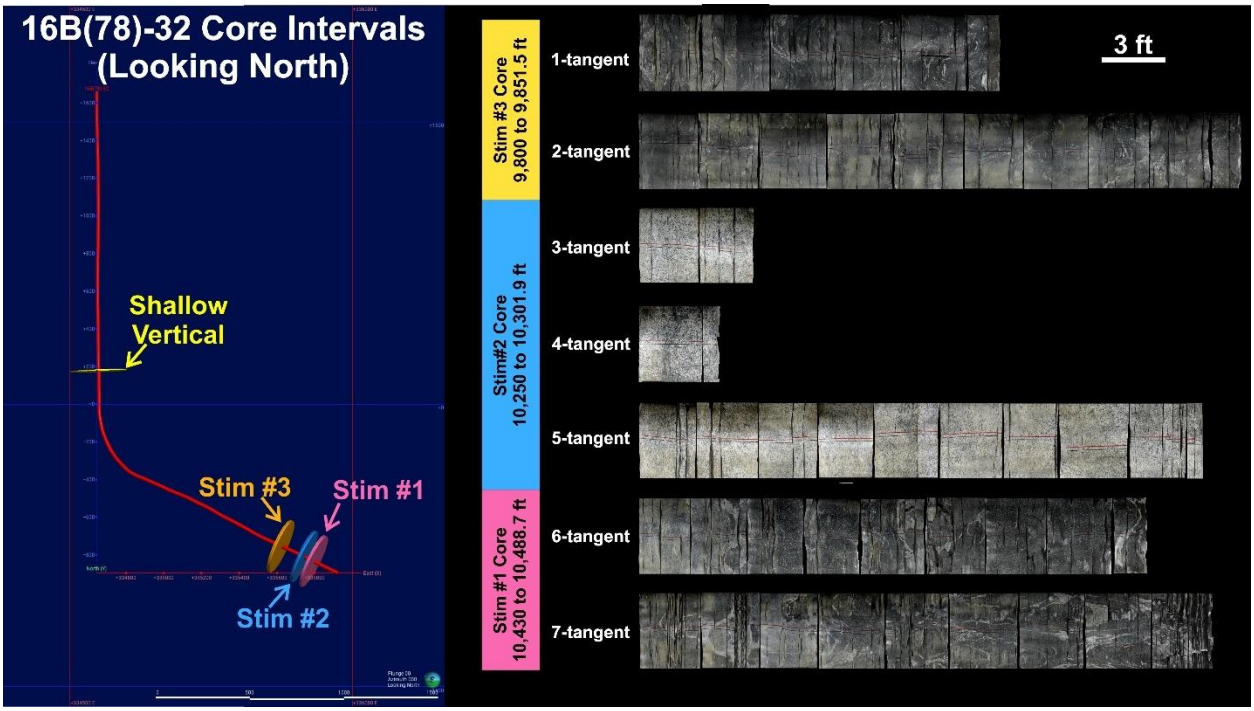

Figure 2: Summary of core collected from the tangent section of 16B(78)-32. In the lefthand image the trajectory of 16B(78)-32 is shown in red with flat disks of appropriate thickness showing the top and bottom measured depths of each core run (the shallow core from the vertical section of the well will not be discussed). In the righthand image, flattened images of the circumference of the core exterior are stitched together. The core images are separated by stimulation zone and core run.

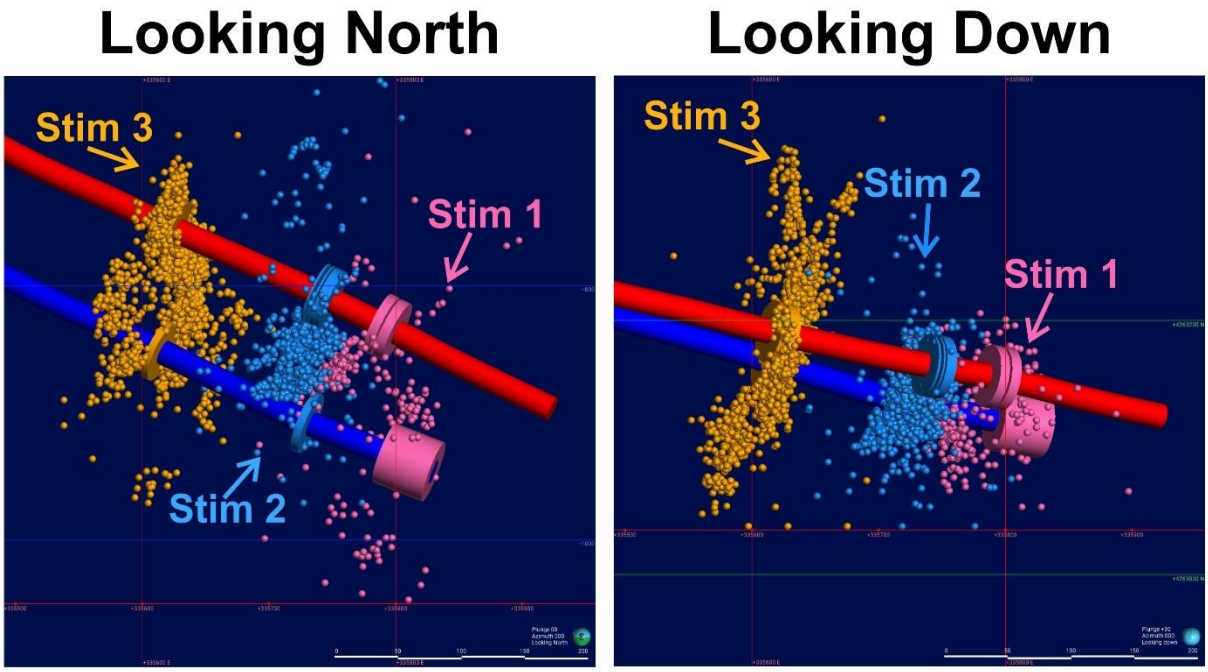

Figure 3: Two perspectives of the toes of wells 16A(78)-32 (blue) and 16B(78)-32 (red) looking to the north at depth (left) and from above (right). Disks on well 16A(78)-32 represent the open hole at the toe, and the perforated intervals above. Disks on 16B(78)-32 represent the seven core runs. Spheres are located seismic events. Symbols are color coded by stage.

1.3 Fracture Morphologies

Fracture morphology categories (Table 2) are, in part, based on previous core characterization reports from core through studies in shales (e.g. Gale et al., 2021), but modified according to observations in the crystalline rocks from Utah FORGE. Orientations were measured for planar, semi-planar, and unbroken mineralized fractures, as well as a single measurement for a thin, compositionally distinct feature (from the stimulation 2 core) that may represent a dike or mylonite. It was not possible to collect measurements from nonplanar features like rough, curviplanar of concave-convex fractures; however, curviplanar and concave-convex features were dominantly perpendicular to the axis of the core. Evidence of abrasion of the core fragments against one another is commonly observed. The impact of mechanical abrasion ranges from parts of fractures being worn smooth/polished, to wearing of the abutting core fragments by differential rotation into smooth concave-convex morphologies, or rubblized sections of the core consisting of rounded rock fragments. Rough, concave-convex and curviplanar fractures (with the exception of those at the bottom of the stimulation 1 core, discussed below) are likely drilling induced, or the result of core handling.

Table 2: Morphologic categories assigned to fractures observed in the 1B(78)-32 core and their possible origins.

Category	Possible origins
Planar	Compatible with natural or induced fractures
Semi-planar	Compatible with natural or induced fractures
Unbroken Mineralized	Natural fractures and/or sealed induced fractures
Rough	Likely the result of coring and/or sample handling
Curviplanar	Drilling induced/core handling or features in the reservoir
Concave-convex	The result of wear caused by differential rotation in the core barrel

1.4 Orienting the Core

The core recovered from well 16B(78)-32 was not oriented and scored during the course of drilling. To orient the core, features observed in the core were correlated, where possible, with features in the Formation Microimager (FMI) log to establish an alignment between coring and logging depths (Table 3). Fractures in the core from stimulation zones 3 and 2 were confidently correlated with features in the FMI logs; however, correlations have yet to be made in the depth interval of stimulation 1. Depth shifts have been applied to core images and core measurements presented in several subsequent figures to match the FMI logging depths.

Planar features in the core were measured while the core was lying horizontally, with the axis of the core having a downhole azimuth of 42°. The planar measurements were then rotated along vertical and horizontal axes to match the azimuth and inclination data recorded in the directional survey of well 16B(78)-32. An axial rotation was then applied to the planar measurements to resemble the fracture orientations interpreted from the FMI log at corresponding depths to approximate the orientations of the fractures in the subsurface prior to coring (Table 3).

Table 3: Summary of depth shifts (+ indicates that the coring depth was shifted downhole to match the FMI logging depth), and rotations applied to the planar measurements from the core to orient the core in situ.

Stimulation Zone	Core Run	Depth Shift (ft)	Horizontal Axis Rotation (°)	Vertical Axis Rotation (°)	Axial Rotation (°)
3	1-T	+10.5	61	24	120
3	2-Ta	+13.1	61	24	115
3	2-Tb	+13.1	61	24	300
2	3-T	+8.4	58	26	N/A
2	4-T	+8.4	58	26	180
2	5-T	+8.1	58	26	75
1	6-T	N/A	N/A	N/A	N/A
1	7-T	N/A	N/A	N/A	N/A

1.5 Coherent Measurements of Fracture Orientations

Coherent sets of planar fracture measurements were made by aligning the core within each 3 ft length of the sectioned core barrel, and between adjacent 3 ft sections within a core run by matching rock fabrics, saw cuts and/or tool marks. Where coherent fracture measurements could not be made within a core run, data sets are denoted by a subscript (i.e. 2-Ta and 2-Tb both come from tangent core run 2). Documentation supplemental to this report is available via the Geothermal Data Repository (Jones, 2025; https://gdr.openei.org/submissions/1708), and includes: 1) flattened images of the core circumference with annotated fractures and depths; and 2) spreadsheets with fracture morphologies by depth; mineralized fractures by depth, as measured planar features; and the orientations of rotated planar features as presented.

1.6 Vein Mineralization

Fractures coated with vein mineralization, fractures partially cutting veins, and unbroken mineralized fractures are common in the 16B(78)-32 stimulation 3 and 1 cores. The veins range from 1 cm in thickness to extremely thin coatings on broken surfaces. Unbroken mineralized fractures have apertures of 2 mm or less. Application of a 10% HCl solution to the core was incredibly useful in detecting the presence of nearly imperceptible coatings of incipient, secondary calcite. Calcite when exposed to this acidic solution dissolves and releases CO_2, resulting in vigorous effervescence. The acidic solution was applied to both broken fracture surfaces and the exterior of the core (where unbroken mineralized fractures were exposed, and other intervals along the exterior of the core). No effervescence was observed on the core exterior where no veins are present.

2 RESULTS

A summary of fracture morphology counts by core interval, as well as counts of mineralized fractures by morphology and core interval are presented in Figure 4. Figure 5 is a legend that shows symbols used to denote morphologic categories assigned to fractures, the presence or lack of vein mineralization in fractures, and the types of fractures interpreted from the FMI log that are used in the subsequent figures presented.

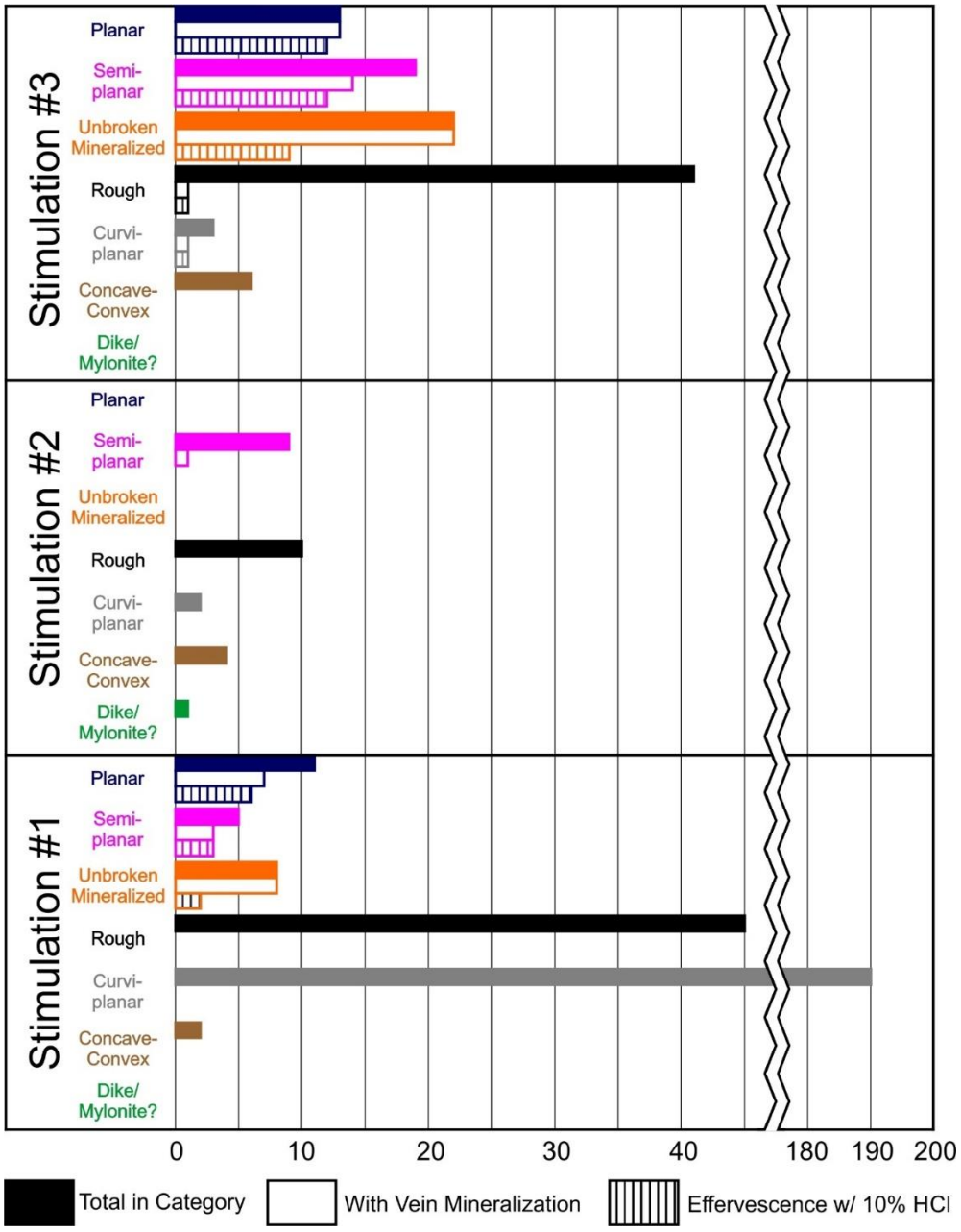

Figure 4: Counts of fracture types observed by morphological category, and core interval with additional data on observations of vein mineralization. Effervescence with application of a 10% HCl solution indicates the presence of calcite.

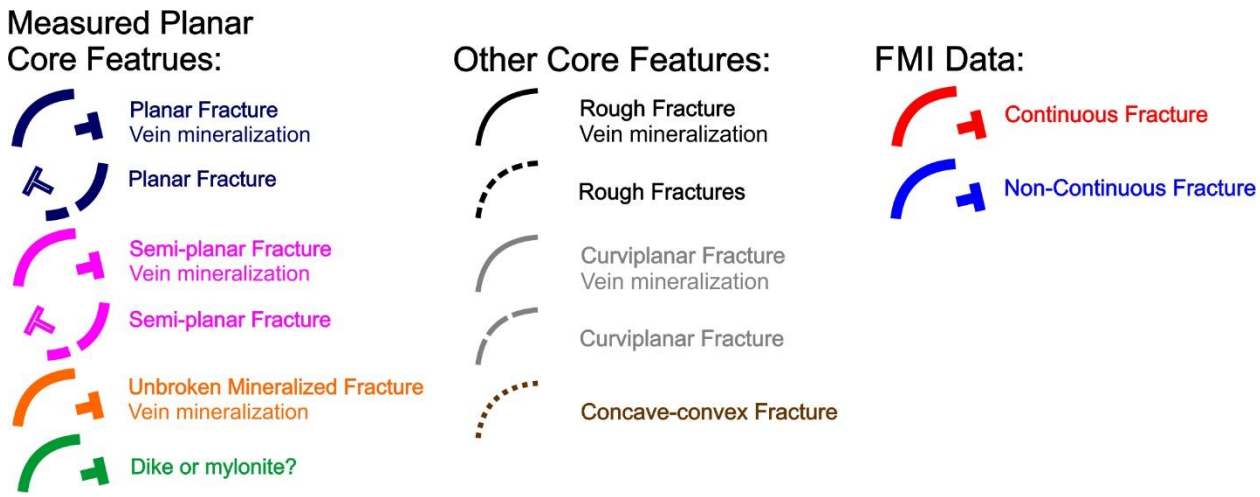

Figure 5: Symbols used to denote morphologic categories assigned to fractures, the presence or lack of vein mineralization in fractures, and the types of fractures interpreted from the FMI log that should be referenced when examining the remaining figures presented.

2.1 Stimulation 3 Core

Two anomalously thick veins, with apertures of up to 1 cm, that contain open cavities lined with euhedral crystals projecting into open space that do not appear to be interconnected were used to correlate drilling and logging depths. These thick veins with remnant open-space match with prominent conductive features in the FMI log at ~ 9,839.5 and 9,845 ft (Figure 6).

The stimulation 3 core contains the most abundant planar features (planar, semi-planar and unbroken mineralized fractures), the vast majority of which contain vein mineralization (Figure 4). Planar features and mineralized fractures are more common in the upper part of tangent core run 1 (Figure 6). Planar features are more evenly distributed in tangent core run 2, with mineralized fractures again more common at shallower depths. Sets of closely spaced unbroken mineralized fractures occur only in tangent core run 2.

Both fractures interpreted from the FMI log, and fractures in the stimulation 3 core (Figure 7) have an overall trend of striking NNE-SSW, in alignment with the regional/local maximum horizontal stress (Handwerger and McLennan, 2019; Xing et al., 2022), and are generally steeply dipping. There are two distinct fracture set orientations in tangent core run 2, one trending NNW-SSE and the second NNE-SSW. Both orientations contain unbroken mineralized fractures as well as broken planar and semi-planar fractures.

2.2 Stimulation 2 Core

A depth correlation was made between coring and logging depths by aligning three pairs of (bifurcated?) semi-planar fractures in the tangent 5 core run with similarly spaced, conductive features in the FMI log (Figure 8). Core from stimulation 2 contained relatively few fractures compared to the core runs above and below (Figures 4 and 8). Fractures in this core interval generally strike NNE-SSW (Figure 9) and are steeply dipping (Figure 8 and 9), in alignment with the local stress field. The single fracture that intersected a mineralized vein has a slightly different trend than the rest, striking NNW-SSE (Figure 9).

2.3 Stimulation 1 Core

The stimulation 1 core has not been confidently matched to features in the FMI log, and therefore no rotations have been applied to the measurements. Unfortunately, the lighter-colored felsic bands in the gneissic core are not distinguishable in the FMI logs. Planar features (planar, semi-planar and unbroken mineralized fractures) are less abundant than in stimulation 3 core, but more abundant than in stimulation 2 core (Figure 4).

In the lower half of tangent core run 7 there are many, regularly spaced (up to 18/ft) curviplanar fractures (Figure 10) that are oriented perpendicular to the core axis (and the trajectory of the well). They are often cohesive (i.e. still stuck together), and the fractures may, or may not, be visible around the circumference of the core. No obvious mineralization was observed on the curviplanar fracture surfaces (either those that were broken in the core barrel, or in cohesive core fragments that were pried apart). Two planar fractures near the bottom of tangent core run 7 (Figure 10) that run nearly parallel to the core axis are coated with incipient calcite. These calcite-coated planar fractures terminate at, and are deflected by, the closely spaced curviplanar fractures (Figure 11).

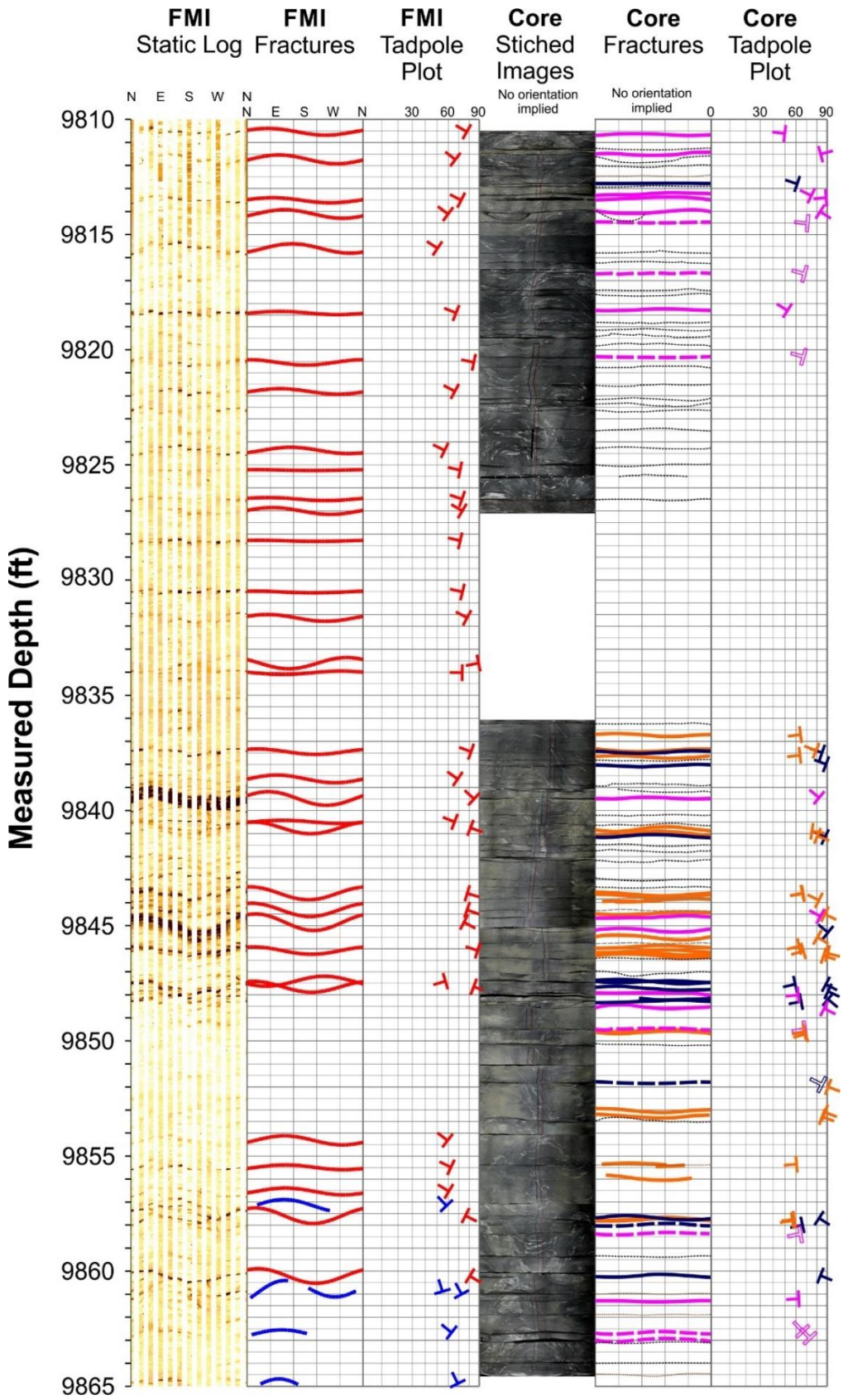

Figure 6: Comparison of FMI image logs and the stimulation 3 core after depth shift and rotations. From left to right: static FMI image log; FMI interpreted fracture traces; FMI fracture orientations; flattened images of the core showing a 360° views of the core's exterior; interpreted fractures in the core; core fracture orientations after rotations were applied.

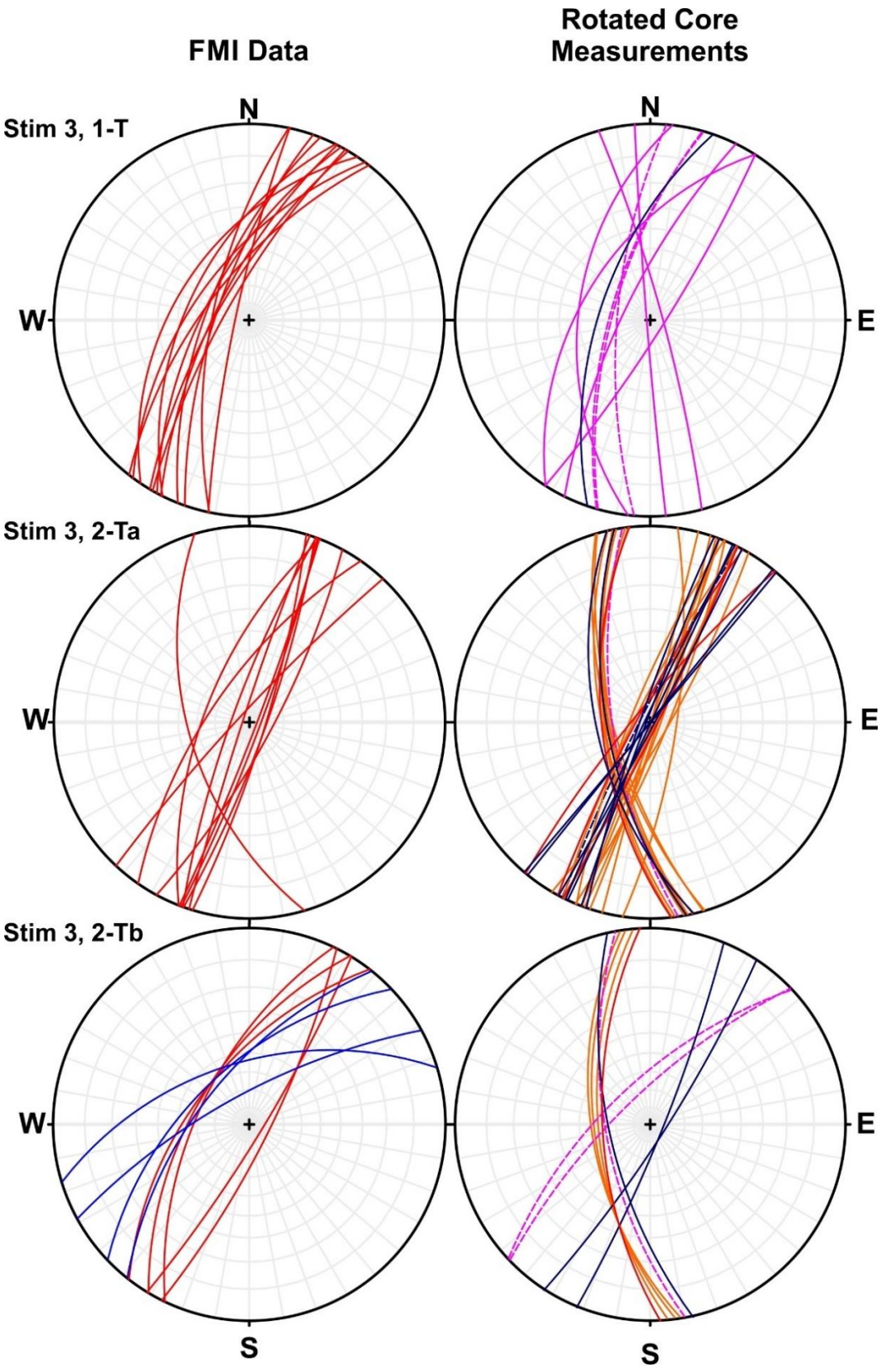

Figure 7: Comparison of planar features interpreted from the FMI logs (lefthand column) and those from the stimulation 3 core after depth shifts and rotations are applied (righthand column). Data sets are separated by cohesive planar measurements (rows). Planes are plotted in lower-hemisphere, equal area, polar grid (10°) stereonets. Data plotted using Stereonet software (Allmendinger et al., 2012; Cardozo and Allmendinger, 2013). See Figure 5 for legend.

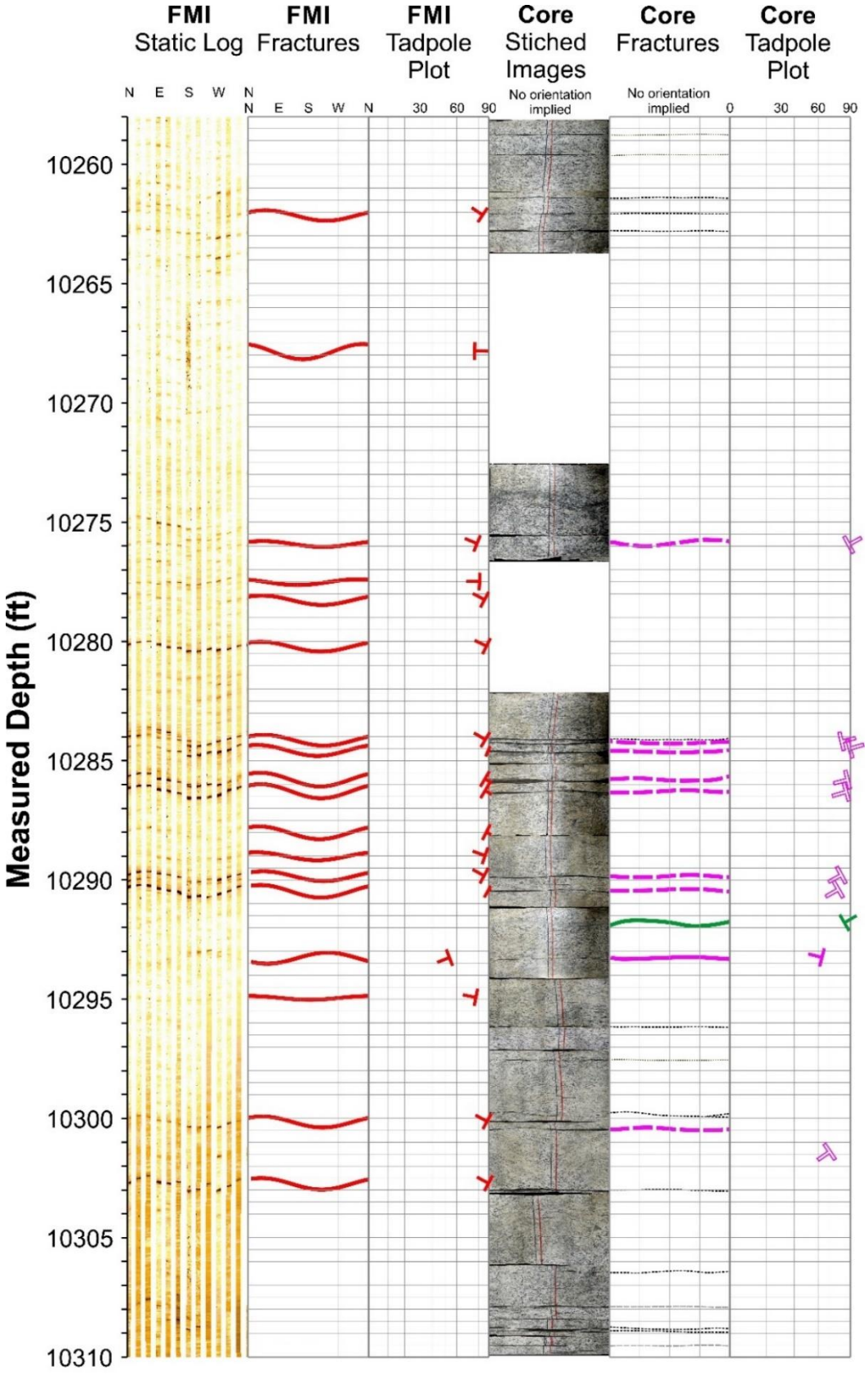

Figure 8: Comparison of FMI image logs and the stimulation 2 core after depth shift and rotations. From left to right: static FMI image log; FMI interpreted fracture traces; FMI fracture orientations; flattened images of the core showing a 360° views of the core's exterior; interpreted fractures in the core; core fracture orientations after rotations were applied.

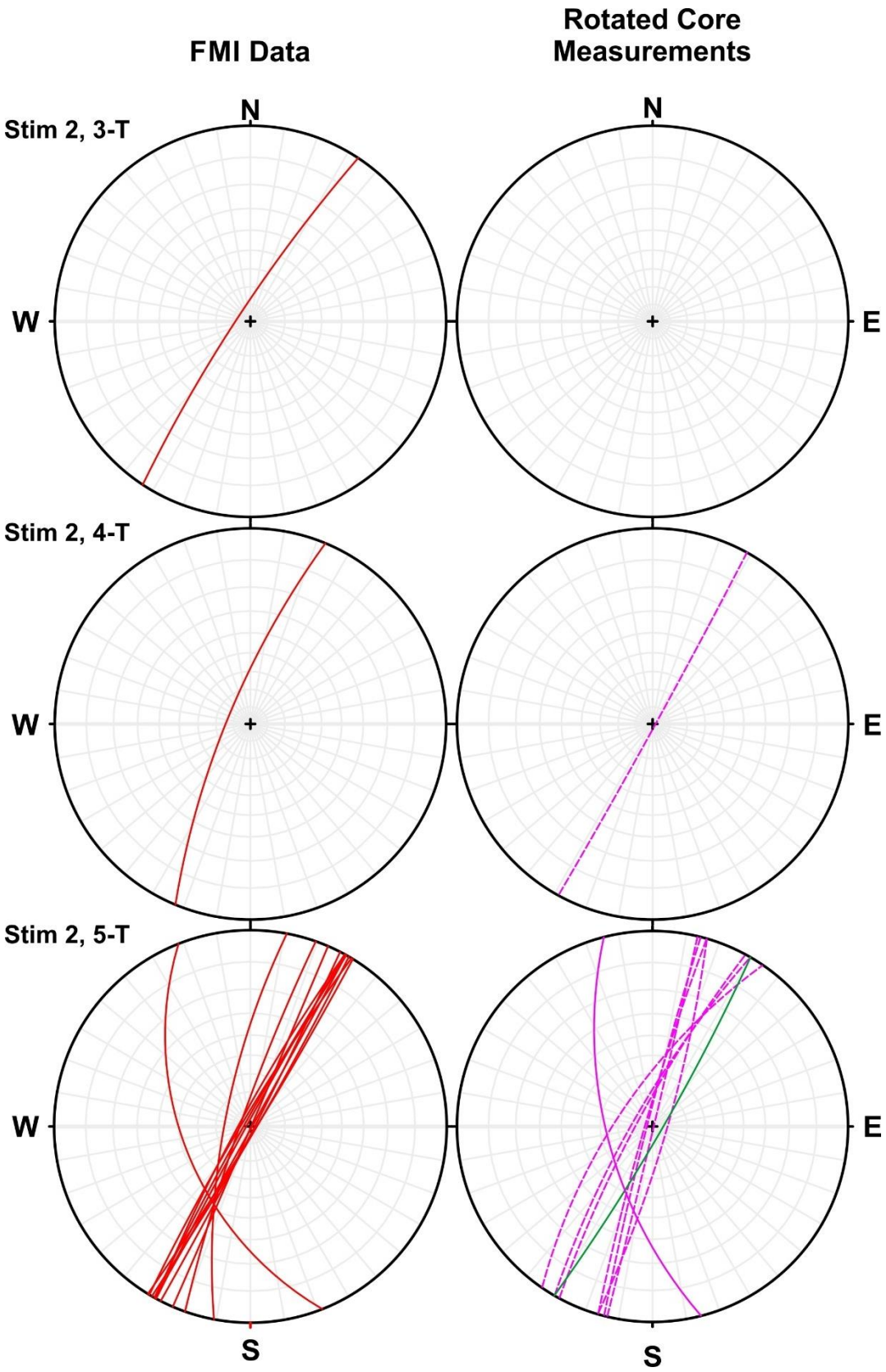

Figure 9: Comparison of planar features interpreted from the FMI logs (lefthand column) and those from the stimulation 2 core after depth shifts and rotations are applied (righthand column). Data sets are separated by cohesive planar measurements (rows). Planes are plotted in lower-hemisphere, equal area, polar grid (10°) stereonets Data plotted using Stereonet software (Allmendinger et al., 2012; Cardozo and Allmendinger, 2013). See Figure 5 for legend.

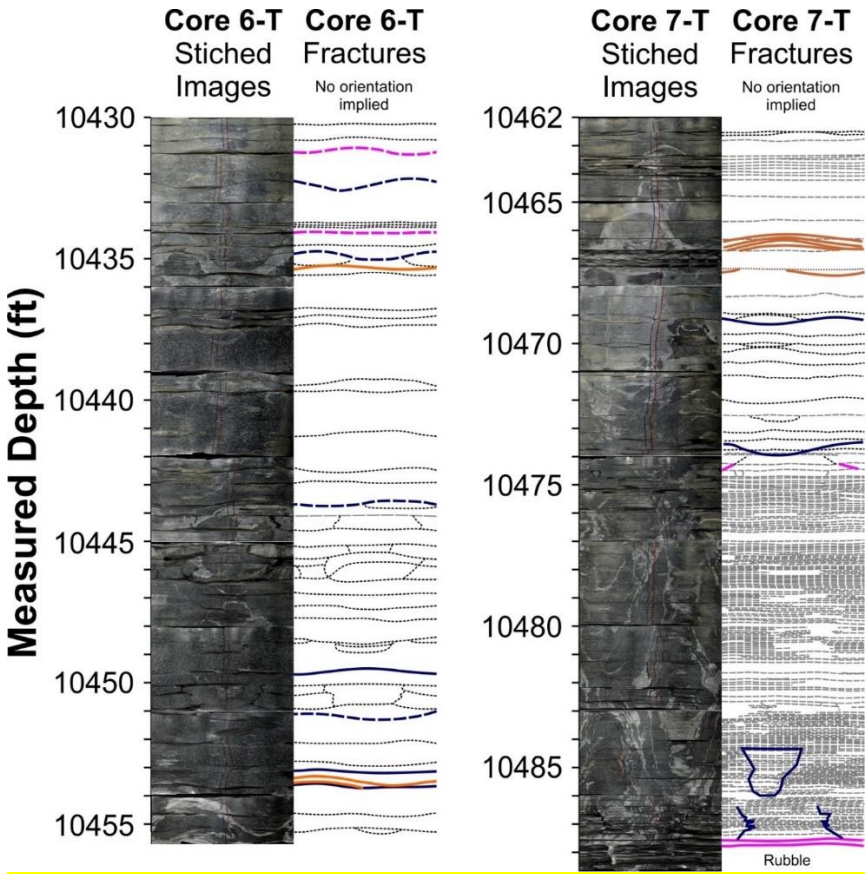

Figure 10: Flattened images of the core showing a 360° view of the exterior of the stimulation 1 core, with adjacent annotations showing fracture locations and geometries. See legend in Figure 5.

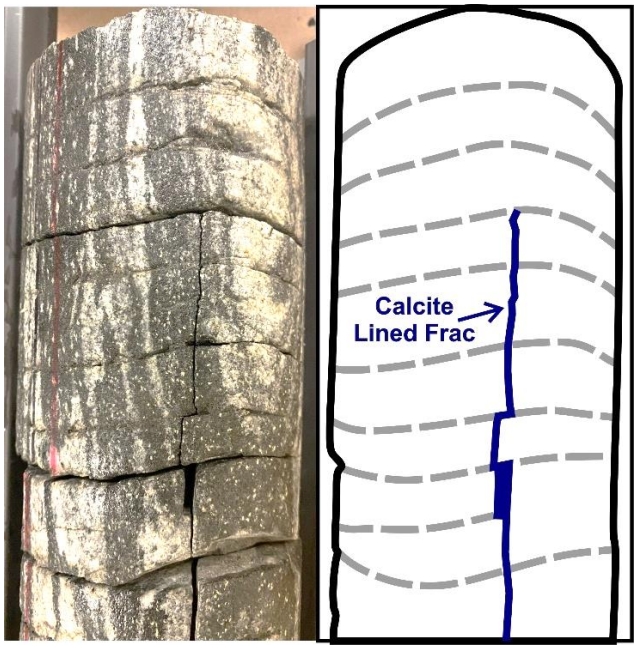

Figure 11. At right is a photograph of a section of the stimulation 1 core from 10,486.43 (at top) to 10,487 ft MD. The core is 4" in diameter. At left is a line drawing of the fractures in the core, with closely spaced curviplanar fractures perpendicular to the core, and a planar fracture, lined with incipient calcite, that terminates at, or is deflected by the curviplanar fractures.

3 DISCUSSION

Planar features (planar, semi-planar and unbroken mineralized fractures) are more abundant in the finer-grained, dark-colored, banded, gneiss in the stimulation 3 and 1 core than in the coarser-grained, light-colored granitoid from stimulation 2 (Figures 2 and 4). Unbroken mineralized fractures and open mineralized fractures were dominantly observed in the gneiss core from stimulations 3 and 1 core as well, with only a single mineralized fracture observed in the stimulation 2 granitoid core.

Mechanical abrasion between core fragments in the core barrel destroyed features in the core. At least two fractures from the stimulation 3 core, with rough and curviplanar morphologies, and evidence of significant wear contained subtle remnants of calcite (Figure 4).

The stimulation 3 core contains the most abundant planar, semi-planar and unbroken mineralized fractures, with the majority of broken planar and semi-planar fractures coated with secondary mineralization (Figure 4). Stimulation 3 core comes from within a planar-shaped seismic cloud where the most microsiesmic events were intercepted by the 16B(78)-32 wellbore (Figure 3); however, it should be noted that there were issues with microsiesmic data acquisition during the stage 2 and 1 stimulations (Dyer et al., 2023a). Stimulation 3 differs from the other two stages in that a viscosifier was added to the treating fluid (stages 2 and 1 used slickwater). There is also evidence for fracture zones in the geophysical well logs both near the stimulation 3 core in 16B(78)-32 and the perforated interval in 16A(78)-32. There is a fracture zone just up hole from the stimulation 3 core, marked in the 16B(78)-32 geophysical logs by decreased resistivity, increased porosity and travel time and contrasting densities above and below. There is also a strong geophysical response from the vicinity of the perforated interval in 16A(78)-32 marked by decreased resistivity and density and increased travel time and porosity. These observations may indicate that stimulation 3 reactivated a preexisting fracture zone linking the injection-production wells at these depths.

Both fractures interpreted from the FMI logs, and rotated fractures measured in the stimulation 3 and 2 core generally strike NNE-SSW and are steeply dipping, in alignment with the stress field. Induced fractures are expected to propagate in a similar orientation.

Work is ongoing to characterize the open-space filling mineralization in the core; however, there appear to be at least three mineral assemblages: 1) actinolite + epidote; 2) Fe- and Mg-bearing carbonates ± quartz ± chlorite ± celestine; and 3) calcite ± anhydrite.

Both actinolite and epidote are expected to precipitate at temperatures well above modern measured temperatures (especially actinolite at ≥ 300°C; Henley and Ellis, 1983) and are interpreted as having formed when the reservoir rock was at greater depth and higher temperature (Jones et al., 2024).

The two large aperture fractures from the stimulation 3 core are dominantly filled by saddle dolomite with curved crystal faces and cleavage planes. Saddle dolomite has been described from sedimentary exhalative deposits (SEDEX) and Mississippi Valley Type (MVT) Pb-Zn ore deposits, as well as ‘hydrothermal dolomite’ hydrocarbon reservoirs. In these environments saddle dolomite has been interpreted to have precipitated rapidly from over pressurized, hot brines in extensional and strike slip tectonic environments and above basement highs that provide pathways for upwelling fluids (e.g. Davies and Smith, 2006). Fe- and Mg-bearing dolomites have been observed in fracture zones from other wells (although not with the saddle dolomite texture). The water used in the stimulations contained little Mg or Fe (Jones et al., 2023), and these fluids are not a likely source for the deposition of relatively thick veins of Mg- and Fe-bearing carbonate, they are therefore interpreted as preexisting natural fractures.

The majority of planar and semi-planar fractures are coated with calcite, and many of the unbroken fractures contain calcite as well, as can be seen by the number of which effervesce when 10% HCl is applied in Figure 4. Calcite coating on fracture surfaces ranges from macroscopic, intergrown calcite and anhydrite, to imperceptible coatings of incipient calcite that is difficult to detect even under a binocular microscope. Similar calcite-and anhydrite-bearing veins have not been observed in other core samples from the Utah FORGE reservoir (although calcite and anhydrite have been observed as minor components of vein mineral assemblages). The minuscule volume of calcite ± anhydrite vein mineralization in relation to the total rock volume recovered in the core samples would be difficult to detect in drill cuttings. It is possible that calcite and anhydrite precipitated from the fluids injected into the reservoir between the stimulation of 16A(78)-32 in April 2022, and when the core was collected in May-June of 2023, over a year later. 10,062 bbl were injected during stimulation, with 6,240 bbl flowed back to the surface, and 3,822 bbl remaining in the reservoir (Jones et al., 2023). Speciation calculations using Geochemists Workbench show that water injected during the stimulations becomes supersaturated with respect to calcite and anhydrite at 30°C and 190°C, respectively.

The closely spaced curviplanar fractures oriented perpendicular to the borehole at the bottom of the stimulation 1 core are interpreted as features in in the reservoir (i.e. they do not appear to be drilling induced, or the result of core handling). The termination and deflection of the perpendicular striking, calcite-bearing veins at, or around the curviplanar fractures, without offset of the rock fabric (Figure 11), suggests that the curviplanar fractures predate the calcite bearing fractures. This also suggests the curviplanar fractures were not permeable, while the calcite-coated, planar fractures were.

4 CONCLUSIONS

Planar features (planar fractures, semi-planar fractures, and unbroken mineralized fractures) generally align with both the regional stress field, and fractures interpreted from the FMI logs. Planar features are more abundant in the gneissic cores from stimulations 3 and 1, than in the granitic core from stimulation zone 2. Mineralized fractures are also more abundant in the gneissic cores.

The stimulation 3 core contained both the most planar features and the most mineralized fractures. Possible contributing factors to the observed fracture distribution include: 1) stimulation 3 was the only stage in which a viscosifier was added to the treating fluid; 2) the microseismic signal was the strongest from stimulation 3 (at least in part due to equipment failures) forming a planar cloud of events

intersected by the 16B(78)-32 wellbore; and 3) geophysical logs suggest that a preexisting fracture zone may have been reactivated to link the injection and production wells.

Calcite ± anhydrite in the core fractures may have been deposited in response to the 2022 stimulation program. The majority of broken fractures are coated with calcite ± anhydrite, to varying degrees, especially in the stimulation 3 core. Both calcite and anhydrite are expected to precipitate from the water injected during stimulations at elevated temperatures.

Cross-cutting relationships suggest the closely-spaced, curviplanar fractures at the bottom of the stimulation 1 core are features in the reservoir that were not permeable.

Attributing an origin to the fractures (i.e. stimulation induced tensile fractures vs preexisting natural fractures vs fractures resulting from drilling or core handling) is difficult, as is making inferences on the timing of fracture development where there are no cross-cutting relationships. At this point all that can be said with certainty is that fractures containing secondary vein minerals were open and filled with fluid in the reservoir prior to the drilling of 16B(78)-32. Future work will be directed at resolving the timing of fracture development and the origin of fluid responsible for vein mineral deposition.

ACKNOWLEDGMENTS

Funding for this work was provided by U.S. Department of Energy under grant DE-EE0007080 “Enhanced Geothermal System Concept Testing and Development at the Milford City, Utah FORGE Site”. We thank the many stakeholders who are supporting this project, including the Utah Geological Survey, the Utah Trust Lands Administration, and Beaver County.

REFERENCES

Allmendinger, R. W., Cardozo, N., and Fisher, D.: Structural geology algorithms: Vectors and tensors in structural geology: Cambridge University Press (2012).

Cardozo, N., and Allmendinger, R.W.: Spherical projections with OSXStereonet: Computers & Geosciences, 51, (2013), 193-205, doi:10.1016/j.cageo.2012.07.021.

Davies, G.R. and Smith Jr, L.B.: Structurally controlled hydrothermal dolomite reservoir facies: An overview. AAPG bulletin, 90(11), (2006), 1641-1690.

Dyer, B.C., Bethmann, F., Karvounis, D., Meier, P., Pankow, K.L., Wannamaker, P., Moore, J., Rutledge, J., Ammon, A.: Innovative microseismic monitoring tools and configurations for geothermal applications. In: Proceedings of the World Geothermal Congress. Beijing, China, (2023a).

Dyer, B., Karvounis, D., Bethmann, F.: Microseismic event catalogues from the well 16A(78)-32 stimulation in April, 2022 in Utah FORGE http://dx.doi.org/10.31905/52CC4QZB (2023b).

Gale, J.F.W., Elliott, S.J., Rysak, B.G., Ginn, C.L., Zhang, N., Myers, R.D. and Laubach, S.E.: December. Fracture description of the HFTS-2 slant core, Delaware Basin, West Texas. In Unconventional Resources Technology Conference, 26–28 July 2021 (2021), 1122-1133.

Handwerger, D.A., and McLennan, J.D.: Wireline log and borehole image interpretation for FORGE well 58-32, Beaver County, Utah, and integration with core data, in Allis, R., and Moore, J.N., editors, Geothermal characteristics of the Roosevelt Hot Springs system and adjacent FORGE EGS site, Milford, Utah: Utah Geological Survey Miscellaneous Publication 169-M, (2019), https://doi.org/10.34191/MP-169-M.

Henley, R. W., and Ellis, A. J.: Geothermal systems ancient and modern: a geochemical review. Earth-science reviews, 19(1), (1983), 1-50.

Jones, C., England, K., Simmons, S., Rose, P., Mella, M., Barker, B., McLennan, J., and Moore, J.: Stimulation, Tracers and Geochemistry at Utah FORGE. Proceedings 48th Workshop on Geothermal Reservoir Engineering, Stanford University, Stanford, CA (2023).

Jones, C., Simmons, S. and Moore, J.: Geology of the Utah Frontier Observatory for Research in Geothermal Energy (FORGE) Enhanced Geothermal System (EGS) Site. Geothermics, 122, (2024).

Jones, C.: Utah FORGE: Well 16B(78)-32 Drill Core Fracture Analysis Images and Data. https://gdr.openei.org/submissions/1708 (2025).

McLennan, J., Mock, B., Swearingen, L., Baldwin, R., Hodder, M., Vetsak, A., Kuhns, A.T., Breland, J., and England, K.: Utah FORGE: Well 16B(78)-32 Drilling Data. United States: Web. doi: 10.15121/1998591 (2023).

Moore, J., McLennan, J., Pankow, K., Simmons, S. Podgorney, R., Wannamaker, P., Jones, C., Rickard, W., and Xing, P.: The Utah Frontier Observatory for Research in Geothermal Energy (FORGE): A laboratory for characterizing, creating and sustaining Enhanced Geothermal Systems. Proceedings 45th Workshop Geothermal Reservoir Engineering, Stanford University, Stanford, CA, (2020).

Moore, J., McLennan, J., Pankow, K., Podgorney, R., Rutledge, J., Meir, P., Byer, B., Karvounis, D., Bethmann, F., Xing, P., Barker, B., Jones, C., Simmons, S., Damjanac, B., and Finnila, A.: Current Activities at the Utah Frontier Observatory for Research in Geothermal Energy (FORGE). Proceedings World Geothermal Congress, Beijing, China (2023).

Xing, P., Wray, A., Velez-Arteaga, E.I., Finnila, A., Moore, J., Jones, C., Borchardt, E. and McLennan, J.: In-situ stresses and fractures inferred from image logs at Utah FORGE. In 47th Workshop on Geothermal Reservoir Engineering, Stanford University, Stanford, CA (2022).